Metabolism of Sirolimus and Its Derivative Everolimus by Cytochrome P450 3A4: Insights from Docking, Molecular Dynamics, and Quantum Chemical Calculations

Bernd Kuhn,[†] Wolfgang Jacobsen,[‡] Uwe Christians,[‡] Leslie Z. Benet,[‡] and Peter A. Kollman*[,†]

Department of Pharmaceutical Chemistry and Department of Biopharmaceutical Sciences, University of California at San Francisco, San Francisco, California 94143-0446

Received February 21, 2001

A combination of quantum chemical calculations and molecular simulations (DOCKing and molecular dynamics) is used to investigate the metabolism of sirolimus (rapamycin) and its derivative everolimus (SDZ-RAD) by cytochrome P450 3A4. Both molecules are drugs with high immunosuppressive activity. Our calculations yield qualitative predictions of the regiospecificities of the hydroxylations and *O*-dealkylations occurring in these two substrates which are in good agreement with recent experimental results. An analysis of the modeled enzyme−substrate interactions allows us to rationalize the reduced metabolic activity of the larger substrate everolimus compared to sirolimus. Moreover, our simulations suggest that hydrogen donor functionalities close to the metabolic site are important for anchoring the substrate at the active center of the enzyme. In particular, we predict that replacing one hydroxyl group by a fluorine atom should considerably suppress the major metabolic reaction in sirolimus, 39-*O*-demethylation.

I. Introduction

The macrolide immunosuppressant sirolimus (rapamycin) was recently approved by the United States Food and Drug Administration for the prophylaxis against graft rejection in kidney transplant patients in combination with cyclosporine.[1] In contrast to the calcineurin inhibitor cyclosporine, which acts early after T-cell activation, sirolimus exerts its action later in the cell cycle by blocking growth-factor driven cell proliferation resulting in synergistic immunosuppressive activity of both drugs.[2,3] The clinical management of sirolimus, however, is complicated by its low and highly variable oral bioavailability.[4] To overcome the formulation problem, the 40-*O*-(2−hydroxyethyl) derivative of sirolimus, everolimus (SDZ-RAD),[5] has been developed and found to have similar immunosuppressive properties[6] but a significantly better oral bioavailability than sirolimus.[7] The significance of cytochrome P450 (CYP) 3A4/5-mediated intestinal and hepatic first-pass metabolism for the oral bioavailability of drugs that are substrates of these enzymes has recently been recognized.[8] As we have previously shown, CYP3A4 is mainly responsible for the metabolism of both sirolimus and everolimus in man.[9,10] CYP3A is also a major source of pharmacokinetic variability of immunosuppressants,[11,12] which has been associated with a high incidence of chronic rejection and poor clinical outcome.[13] Therefore, it is of major interest to investigate and compare the metabolism of sirolimus and everolimus in CYP3A4, which we have done both by experimental and theoretical means. The experimental study[10] identified a total of 12 and 13 metabolic sites in sirolimus and everolimus, respectively, and clustered them into metabolic groups, as illustrated in Figure 1. Groups 1−4 involve hydrocarbon hydroxylation reactions and group 5 contains all *O*-dealkylations occurring in the two substrates. While the total intrinsic clearance of the CYP-dependent formation of everolimus metabolites is 3-fold lower than for sirolimus, some of the metabolic rate constants are found to be drastically reduced by attaching the 2-hy-

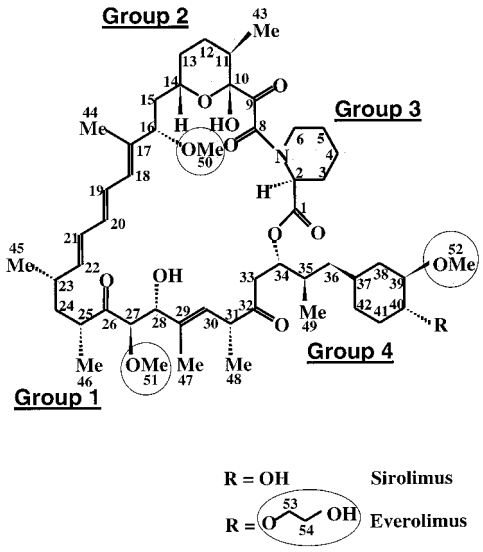

Figure 1. Molecular structure of sirolimus (R = OH) and everolimus (R = O−CH_2−CH_2−OH) including labeling of the carbon atoms. Five metabolic groups, marked by circles, have been identified experimentally in microsomal cytochrome P450's involving hydroxylations (groups 1−4; solid background) and *O*-dealkylations (group 5: Me^{50}-Me,^{52} C^{53}-CH_2−OH; lined background).[10] We have studied groups 1 and 2 and the cyclohexyl-ring of group 5 in CYP3A4. Abbreviation: Me = methyl.

* Author to whom correspondence should be addressed. Tel: 415 476-4637. Fax: 415 476-0688. E-mail: pak@cgl.ucsf.edu.
[†] Department of Pharmaceutical Chemistry.
[‡] Department of Biopharmaceutical Sciences.

10.1021/jm010079y CCC: $20.00
Published on Web 05/11/2001

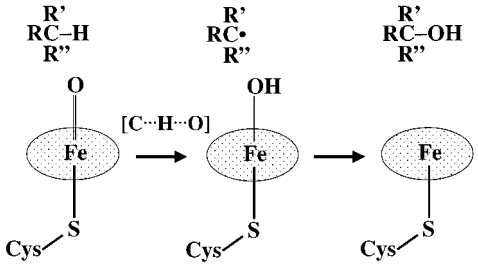

Figure 2. Proposed mechanism for hydrocarbon hydroxylation and *O*-dealkylation (R = R*O) of substrates in cytochrome P450.[15] The transition state for hydrogen atom abstraction, [C···H···O], is assumed to be linear. Cys-S stands for a cysteinate residue, and the tetrachelated porphyrin moiety is represented by a dotted ellipse. Figure modified from ref 15.

droxyethyl group to sirolimus. Most notably, the major metabolism reaction in sirolimus, 39-*O*-demethylation, is slowed by a factor of ≈15 in everolimus. To better understand the molecular basis for the observed behavior and to test whether our theoretical approach can be used in a predictive manner, we have used computational methods to investigate the reactions of the main metabolic groups in CYP3A4. This enzyme was chosen since a three-dimensional (3D) homology model[14] was available for our simulations, and because it is the major human cytochrome P450 involved in drug metabolism.

To theoretically predict the rate constant of a multistep reaction, one has to simulate the rate-limiting step of this process. There is experimental and theoretical evidence[15,16] that for CYP metabolized hydrocarbon hydroxylation and *O*-dealkylation reactions, which are of relevance for sirolimus and everolimus, the rate-limiting reaction involves the two-step radical mechanism illustrated in Figure 2. The first step contains hydrogen atom abstraction from the substrate by the activated heme oxygen of CYP, which is followed by radical recombination to form the hydroxylated molecule. In substrates in which a substituent contains an oxygen atom adjacent to the reaction center, i.e. R = R*O, the hemiacetal formed is not stable under the conditions in the enzyme and decomposes into the dealkylated product and a free aldehyde or ketone, depending on the substituents R′ and R″. Large kinetic isotope effects suggest that hydrogen atom abstraction is rate-limiting and that a linear [C···H···O] transition state is involved in the radical formation.[15]

Ideally, one would like to model the hydrogen abstraction reaction using combined quantum mechanical/molecular mechanical (QM/MM) methods. However, since the available 3D structures of sirolimus/CYP3A4 are not accurate enough to warrant an elaborate QM/MM model we used a qualitative approach instead. Our method is based on the knowledge of the rate-limiting step, i.e. atomic hydrogen abstraction from the substrate (first step in Figure 2), of the reaction and takes into account both electronic effects at the reaction site and interactions between the substrate and CYP3A4. An important factor influencing the reaction rate is the enthalpy change involved in forming the transition state from the reactants. Using the Hammond postulate, this can be approximated by the energy difference between the radical intermediates and the reactant

$$\Delta E = E(\mathrm{R}\bullet) + E(\mathrm{H}\bullet) - E(\mathrm{R{-}H}) \qquad (1)$$

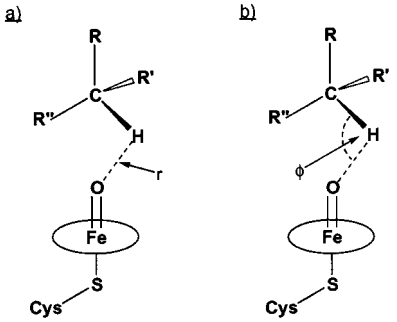

Figure 3. Geometric parameters used in the analysis of enzyme−substrate interactions. The dashed lines show (a) the distance between the heme oxygen atom and the reactive substrate hydrogen atom, *r*, and (b) the angle between those two atoms and the adjacent substrate carbon atom, ϕ.

which, for the same substrate, corresponds to the stability of the formed radical R•. We estimate the propensity of each reaction site to lose a hydrogen atom by quantum chemical calculations of the substrate according to eq 1. Apart from this electronic criterion, one has to consider how interactions between the enzyme and the substrate affect their relative orientation at the active site. This is important because the reaction probability at a given site is highly dependent on the distances and angles of the atoms involved in the chemical transformation. Taking into account substrate−enzyme interactions is clearly necessary for large substrates such as sirolimus and its analogues. We model the intermolecular interactions by molecular dynamics (MD) simulations of the substrate-CYP3A4 complex. Based on the knowledge about the linear transition state during hydrogen atom abstraction, we use as geometric criteria the distance between the reactive substrate hydrogen atom and the ferryl oxygen atom, *r*, as well as the angle between those atoms and the adjacent substrate carbon atom, ϕ. These two geometrical parameters are illustrated in Figure 3. Similar qualitative approaches, pioneered by Loew et al.,[17,18] have been applied with considerable success to predict metabolic product distributions of different substrates in bacterial cytochrome $P450_{cam}$[19−22] and homology models of CYP 2C enzymes.[23,24]

Using the above-mentioned electronic and orientation criteria, we investigate 10 and 11 possible metabolic pathways for sirolimus and everolimus, respectively. The modeled reactions involve the metabolic groups 1 and 2 as well as the *O*-dealkylation reactions at the cyclohexyl-ring (part of group 5), which are the most important in CYP3A4. Experimental rate constants[10] have been measured for all sites studied and provide a good testing ground for our simulations. We distinguish the different metabolic pathways by the substrate carbon atom at which the initial hydrogen abstraction occurs. For *O*-dealkylations this is the carbon atom that is eliminated adjacent to the oxygen atom.

II. Experimental Section

(a) Electronic Structure Calculations. We used the three model compounds depicted in Figure 4 to estimate possible electronic effects on the metabolic rates in groups 1, 2, and 5 of sirolimus and everolimus. The model systems were chosen to include all atoms that are likely to affect the electronic structure at the reaction centers. Hydrogen atom abstraction energies at the labeled positions of Figure 4 were

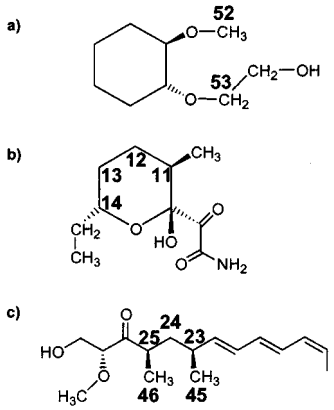

Figure 4. Model compounds used to calculate the hydrogen abstraction energies at the metabolic groups (a) 5 (cyclohexyl-ring), (b) 2, and (c) 1 of sirolimus/everolimus (see Figure 1). Energies of the cyclohexyl-ring of group 5 for sirolimus and its fluoro analogue (see section Results and Discussion) were obtained by substituting R = −O−CH_2−CH_2−OH with R = −OH and R = −F, respectively. The labeled carbon atoms denote the positions for which we calculated hydrogen atom abstraction energies.

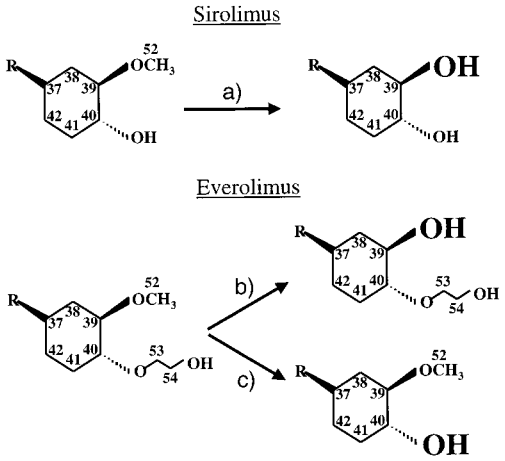

Figure 5. Experimentally identified metabolic pathways at the cyclohexyl-ring of sirolimus and everolimus (part of group 5).[10] The measured rate constants are (a) k = 254 pmol × mg^{-1} × min^{-1} for 39-*O*-demethylation in sirolimus, (b) 5 pmol × mg^{-1} × min^{-1} for 39-*O*-demethylation in everolimus, and (c) 23 pmol × mg^{-1} × min^{-1} for 40-*O*-dehydroxyethylation in everolimus.

calculated with the density functional theory (DFT)/B3LYP (Becke three-parameter Lee−Yang−Parr)[25−27] method using the 6-31G* basis set,[28] with all radicals being treated at the spin-unrestricted level of theory, UB3LYP. The geometries of the reactants and radical intermediates were optimized before energy evaluation. No spin projection was applied to the UB3LYP wave function as this might degrade the calculated energy.[29] A comparison of different quantum chemical methods in describing open-shell systems has shown that UB3LYP/6-31G* calculations yield excellent optimized geometries and relative energies for radicals, comparable to much higher levels of theory, provided that the spin contamination of the wave function is small.[30] We monitored the extent of spin contamination in our open-shell calculations and quote its value in the rare cases when it deviates considerably from the spin of a doublet state, $|S^2| = 0.75$. All electronic structure calculations were performed with the software package Gaussian 98.[31]

(b) Docking and Molecular Dynamics Simulations. Our MD simulations were based on a homology model of CYP3A4 by Szklarz and Halpert which used the crystallographic coordinates of four bacterial CYP enzymes as templates.[14] The two ligands, sirolimus and everolimus, were docked into the active site of the model using DOCK 4.0.[32] This was done in an "anchor-and-grow" fashion independently for each of the three metabolic groups such that the corresponding group center was placed in proximity to the heme oxygen atom. For the subsequent molecular dynamics simulation, we used the standard parm94 force field of AMBER 5[33] together with new parameters for the ligands, which were derived as outlined previously.[34] Atomic partial charges for sirolimus and everolimus were obtained by semiempirical AM1 geometry optimization and subsequent single-point Hartree−Fock/6-31G* calculation of the electrostatic potential, to which the charges were fitted using the restrained electrostatic potential (RESP) procedure.[35] Force field parameters[18,36] and partial charges[20] for the heme unit of CYP3A4, which consists of an iron-oxo porphyrin complex with an axial cysteinate ligand from the protein, were taken from the literature. Throughout the MD simulations, we used a cutoff for nonbonded interactions of 14 Å and allowed only residues within 16 Å of the substrate to move. The SHAKE algorithm[37] was used with an integration time step of 1.5 fs.

Since the six docked structures, three for each substrate, showed significant steric overlap between the protein and the ligand, due to limitations in docking large ring systems, we performed simulated annealing of the ligand in each of those complexes to improve the starting structure for MD. Here, the temperature of the system was first increased from $T = 0$ to 1200 K within 3 ps and reduced again to $T = 0$ K by tightening the temperature coupling, τ_T, from τ_T = 4.0−0.05 ps over a simulation time of 12 ps. Only residues within 16 Å of the substrate were allowed to move, thereby keeping all protein atoms close to their initial positions with a harmonic positional restraint of 20 kcal/(mol Å^2) and the corresponding metabolic group center close to the heme group with an internal harmonic restraint of 200 kcal/(mol Å^2). During this step, we stiffened the torsional potential around all double bonds of the ligand to avoid cis−trans isomerization at the elevated temperatures. Our simulated annealing procedure lowered the complex energies by up to 1300 kcal/mol compared to the initial docking conformation. The root-mean-square deviation between the substrate structures after and before simulated annealing ranged from (0.6−3.4) Å for the six complexes investigated. After annealing, we solvated the ligand−protein complexes with a 25 Å sphere of TIP3P water molecules,[38] centered at the ferryl oxygen atom.

To elucidate the steric effects that affect the metabolic rate at the 10 (sirolimus) and 11 (everolimus) investigated reaction centers (see numbers in Figure 4) we used the following MD protocol for each of the 21 systems. First, we equilibrated the solvated complex for 50 ps at T = 300 K using an internal harmonic restraint of 20 kcal/(mol Å^2) between the heme oxygen atom and the reactive carbon center. The equilibrium distance was set to 3.6 Å, which is the sum of their van der Waals radii. This restraint was applied to ensure that the subsequent unrestrained MD simulation started from an enzyme−substrate configuration that is favorable for reaction. Abolishing the active-site restraint, we then performed 50 ps of additional equilibration and 160 ps of data collection to see whether the modeled enzyme−substrate complex kept this "reactive" configuration in place. We saved the coordinates of the complex every 2 ps, yielding a representative set of 80 structural snapshots for each system. This ensemble of structures was analyzed with respect to the population of the two geometrical parameters shown in Figure 3.

III. Results and Discussion

(a) Group 5. The experimental rate constants for metabolism at the cyclohexyl-ring of sirolimus and everolimus (Figure 5) are drastically different between the two substrates. While 39-*O*-demethylation, which involves initial H-abstraction at C52, is the major metabolism reaction in sirolimus with a rate constant of k = 254 pmol × mg^{-1} × min^{-1}, this metabolic

Table 1. Hydrogen Atom Abstraction Energies, ΔE, at Different Carbon Centers in the Metabolic Groups 5, 2, and 1 of Sirolimus/Everolimus Using the Model Compounds Shown in Figure 4[e]

	group 5[a]
C52[b]	101.2
C53	100.8
	group 2[c]
C11	101.7
C12	104.8
C13	105.3
C14	100.6
	group 1[d]
C23	77.7
C24	102.1
C25	92.1
C45	108.9
C46	107.7

[a] Absolute energy of reactant (Figure 4a): $E_{B3LYP/6-31G^*} = -579.4341305$ hartree. [b] Replacing the substituent R = −O−CH_2−CH_2−OH in the model compound (Figure 4a) with R = −OH and R = −F yields ΔE = 101.8 and 101.2 kcal/mol, respectively. [c] Absolute energy of reactant (Figure 4b): $E_{B3LYP/6-31G^*} = -746.9565938$ hartree. [d] Absolute energy of reactant (Figure 4c): $E_{B3LYP/6-31G^*} = -850.9559417$ hartree. [e] Energies are calculated using the (U)B3LYP/6-31G* method and are given in kcal/mol.

pathway is almost completely blocked in everolimus (k = 5 pmol × mg^{-1} × min^{-1}). As can be seen from Figure 5, another *O*-dealkylation pathway is detected in everolimus, leading to sirolimus, with k = 23 pmol × mg^{-1} × min^{-1}. We modeled these three metabolic routes using the electronic and geometric criteria explained above.

As listed in Table 1, small energetic differences below 1 kcal/mol exist in the calculated stability of the three possible radical intermediates which are unlikely to explain the spread of observed rate constants. To elucidate the effects of substrate−enzyme interactions we analyzed the MD trajectories for sirolimus and everolimus in Tables 2 and 3, respectively. Using the distance between the ferryl oxygen atom and the reactive hydrogen atom as well as the angle between those two atoms and the neighboring carbon atom as critical parameters, we calculated (a) their MD averages and (b) the probability of finding a substrate−enzyme configuration suitable for reaction. We define the geometric criteria of those configurations as r < 2.7 Å, i.e. the distance between the heme oxygen and substrate hydrogen atom should be smaller than the sum of their van der Waals radii, and as $|\phi - 180°| < 45°$. This criterion for the angle was chosen because the reaction probability should be highest when the two reactants approach each other in a linear [C···H···O_{Fe}] configuration, ϕ = 180°, this being the likely arrangement in the transition state. Deviations from the linear orientation should increase the transition state barrier, which is, however, difficult to quantify and was not attempted in our qualitative approach. As a crude measure, we distinguish more "reactive" configurations in which $|\phi - 180°| < 45°$ (class A) and less "reactive" configurations in which $|\phi - 180°| > 45°$ (class B). Table 2 indicates that there is a significant probability (25%, 8%) of finding sirolimus in a configuration relative to the heme group that is favorable for hydrogen atom abstraction at C52, ultimately leading to 39-*O*-desmethyl sirolimus. This number is considerably higher than the probability (3%, 4%) for the same reaction site in everolimus (Table 3), in agreement with the experimental observation of a significantly reduced rate constant in everolimus. Molecular dynamics simulations of the dehydroxyethylation pathway at C53 of everolimus, yielding sirolimus (Figure 5c), reveal that the average distance between the reactive substrate hydrogen atom and the heme oxygen atom is favorable for reaction, but that the average C,H,O_{Fe} angle is considerably bent compared to the optimal linear configuration. This unfavorable angular orientation might be the reason this metabolic pathway is slower than the 39-*O*-demethylation in sirolimus. Our numerical results are illustrated in Figure 6 showing the sampled conformations during the MD calculations. Most noticeably, the distribution of snapshots for the dehydroxyethylation

Table 2. Geometrical Analysis of the Molecular Dynamics Results of CYP3A4 Bound Sirolimus[b]

	$\bar{r}$/Å	$\bar{\phi}$/degrees	A	B	k_{exp}
		Group 5 (*O*-Dealkylation)			
C52[a]	3.2 (0.8)	136 (22)	25	8	254 (7)
		Group 2 (Hydroxylation)			
C11	3.0 (0.2)	102 (6)	0	9	137 (2)
C12	2.8 (0.4)	121 (12)	20	19	109 (3)
C13	4.7 (0.3)	69 (4)	0	0	−
C14	3.2 (0.4)	123 (9)	2	0	45 (5)
		Group 1 (Hydroxylation)			
C23	4.2 (0.3)	87 (11)	0	0	137 (5)
C24	2.8 (0.3)	153 (10)	19	1	
C25	4.2 (0.4)	92 (8)	2	4	107 (1)
C45	2.9 (0.3)	148 (13)	33	3	79 (3)
C46	4.1 (0.5)	110 (12)	12	1	

[a] Replacing R = −O−H with R = −F at position C40 yields $\bar{r}$ = (9.8 ± 1.1) Å and $\bar{\phi}$ = (111 ± 16)°, with no population of the classes A and B. [b] The first column indicates the carbon atom of the substrate to which the reactive hydrogen atom is attached. Columns 2 and 3 list the MD averaged distance between the heme oxygen atom and the reactive H-atom of the substrate, $\bar{r}$, and the average angle of these atoms with the adjacent substrate carbon atom, $\bar{\phi}$, respectively (80 snapshots). When methylene and methyl units are examined, the H-atom closest to the heme oxygen atom is selected for each MD snapshot. Classes A and B denote the probability of sampling a snapshot with A, r < 2.7 Å and $|\phi - 180°| < 45°$, and B, r < 2.7 Å and $|\phi - 180°| \geq 45°$. Here, all trajectories for a given group are taken into account. Experimental rate constants, k_{exp}, in CYP3A4 are listed for comparison (pmol × mg^{-1} × min^{-1}). Numbers in parentheses indicate the standard deviation.

Table 3. Geometrical Analysis of the Molecular Dynamics Results of CYP3A4 Bound Everolimus[a]

	$\bar{r}$/Å	$\bar{\phi}$/degrees	A	B	k_{exp}
		Group 5 (*O*-Dealkylation)			
C52	4.5 (1.6)	114 (19)	3	4	5 (1)
C53	2.5 (0.2)	111 (10)	1	58	23 (2)
		Group 2 (Hydroxylation)			
C11	3.0 (0.2)	97 (6)	0	2	18 (1)
C12	3.8 (1.2)	103 (13)	16	9	20 (1)
C13	3.8 (0.5)	105 (10)	0	0	−
C14	5.6 (0.3)	94 (9)	0	0	7 (1)
		Group 1 (Hydroxylation)			
C23	4.0 (0.3)	142 (14)	0	0	45 (1)
C24	3.0 (0.5)	139 (12)	21	1	
C25	4.0 (0.4)	84 (9)	0	0	23 (1)
C45	3.4 (0.3)	118 (13)	1	1	46 (3)
C46	3.9 (1.1)	128 (16)	23	5	

[a] The nomenclature is described in Table 2.

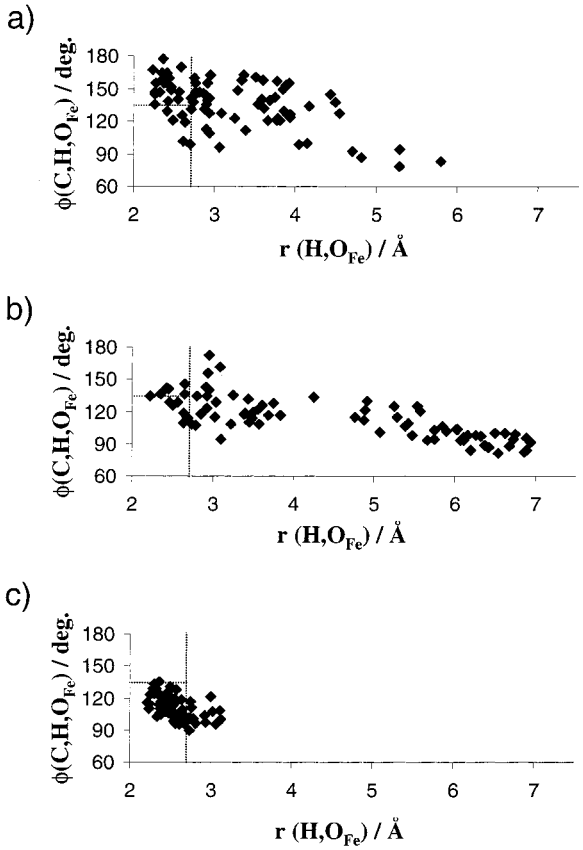

Figure 6. Population of the two critical geometric parameters for reaction, r and ϕ, using individual molecular dynamics simulations for the metabolic sites at the cyclohexyl-ring (part of group 5) of sirolimus and everolimus. The charts display the results for hydrogen abstraction from (a) C52 in sirolimus, (b) C52 in everolimus, and (c) C53 in everolimus. The number of structural MD snapshots is 80. The dashed lines indicate the geometric criteria ($r = 2.7$ Å, $\phi = 135°$) used to distinguish "reactive" from "nonreactive" configurations.

reaction in everolimus (Figure 6c) is more compact than the for the other reactions in this group.

Further insight into the molecular interactions leading to the simulated behavior can be gained by inspecting characteristic MD snapshots of the complex. Figure 1 in the Supporting Information displays the equilibrated structure of the active site of the sirolimus/CYP3A4 complex involving the heme group and the bound substrate. Interestingly, the hydroxyl group adjacent to the OCH_3 group at which demethylation occurs forms a strong hydrogen bond ($d \approx 1.8$ Å) with the negatively charged ferryl oxygen atom. This interaction seems to "anchor" the cyclohexyl-ring of the substrate close to the heme group, thereby forming an eight-membered ring with the ferryl oxygen at an angle $\phi \approx 140°$, which is close to linear. Inserting a CH_2-CH_2-O moiety into the hydroxyl group of sirolimus, as is the case for everolimus, leads in our simulations to the break-up of the substrate-heme ring configuration and floating away of the substrate. Consequently, the displaced OH group of the substrate has to point into the hydrophobic protein environment around the heme group, which is energetically unfavorable. In contrast to the 39-*O*-demethylation of everolimus, the dehydroxyethylation reaction (Figure 5c) involves again the formation of a hydrogen bond between the substrate and the heme oxygen, as displayed in Figure 2 in the Supporting Information. However, in this six-membered ring the relative location of the hydroxyl group and the methylene group at which the initial hydrogen abstraction occurs forces ϕ to adopt a value around 110° rather than $\phi = 180°$.

Our simulations of the *O*-dealkylations at the cyclohexyl-ring of sirolimus and everolimus, which are in qualitative agreement with the experimental results, suggest that hydroxyl functionalities or other hydrogen bond donors close to the reaction center play an important role in providing an "anchor" for the substrate to approach the heme group. To further test this hypothesis, we replaced the OH group at C40 of sirolimus with a fluorine atom, whose negative charge should repel the heme oxygen atom. While the stability of the intermediate radical is little affected by this substitution ($\Delta\Delta E = 0.6$ kcal/mol), the MD simulations revealed a drift of this compound away from the active site. This suggests that the main metabolism in sirolimus, which is 39-*O*-demethylation, could be reduced by the simple substitution of a hydroxyl group with a fluorine atom at C40.

(b) Group 2. Several metabolic sites, involving hydroxylations at the carbon atoms C11, C12, and C14, have been identified experimentally in group 2 for sirolimus and everolimus.[10] The measured rate constants for those pathways are listed in Tables 2 and 3. To test the predictive power of our approach we modeled both the three sites of this group for which metabolites have been found and the site C13 for which no metabolism product was detected.

As expected, our calculations of the energies for hydrogen abstraction (Table 1) reveal two classes of substrate radicals. The tertiary radical intermediates, which are formed at C11 and C14, are 3−5 kcal/mol more stable than the secondary radicals at C12 and C13. Based on the electronic criterion alone, one would deduce that the 11-OH and 14-OH metabolites occur more often than the 12-OH and 13-OH metabolized substrates. However, MD simulations of the substrate-CYP3A4 interactions (Tables 2 and 3) show that in both substrates it is considerably more likely that the C12 carbon atom approaches the heme oxygen in a "reactive" configuration than it is for the other three carbon atoms. This favorable geometry for 12-OH hydroxylation should partly compensate the higher transition state barrier for this pathway compared to the 11-OH and 14-OH hydroxylations. This behavior was found experimentally as listed in the last column of Tables 2 and 3. Encouragingly, our calculations confirm the experimental observation that no 13-OH metabolite should be formed in both substrates. This is due to unfavorable ligand−enzyme interactions, which prevent the substrate C13 atom to come close to the activated heme oxygen.

In all groups, we find that it is generally less likely that a "reactive" configuration is formed in everolimus than in sirolimus, in agreement with the observed trend of smaller rate constants for the bigger substrate everolimus. For the metabolism in group 2, this arises from the fact that the long hydroxyethyl-chain in everolimus is forced to point into the compact protein base around the heme group to permit close encounters of the reactants at the reaction site. Consequently, this leads to some repulsion of everolimus from CYP3A4 and

larger average distances between the metabolic sites and the heme group.

(c) Group 1. In group 1, we investigated possible hydroxylation reactions at the substrate carbon atoms C23−C25 and C45−C46 in both sirolimus and everolimus. Three metabolites have been found experimentally in this group, with some ambiguity in two cases, namely whether (a) 45-OH or 46-OH and (b) 23-OH or 24-OH hydroxylations are involved. Our electronic structure calculations show more variance in the reaction energies than in the other groups, yielding the following order of radical stability: C23 ≫ C25 ≫ C24 > C45, C46. Most noticeable is the relatively small energy change, ΔE = 77.7 kcal/mol, for hydrogen atom abstraction at C23. Although the accuracy of this value might be lower than the others, due to a relatively high spin contamination ($|S^2| = 0.81$) of the radical, the large stabilizing effect of the conjugated π-bond system adjacent to C23 on the radical intermediate should make hydrogen abstraction at this atom electronically much more favorable than at the other sites. However, as the MD simulations on the substrate/CYP3A4 complexes show, the hydrogen atom attached to C23 never comes close to the heme oxygen atom, thereby preventing metabolism at this site. Apparently, the extended polyene chain has two opposite effects on the adjacent carbon atom C23. While it stabilizes considerably the radical intermediate that is formed during the reaction, the low chain flexibility makes it difficult to accommodate this substrate segment close to the heme group without having unfavorable interactions with neighboring protein residues. Our simulations suggest that in sirolimus hydroxylation reactions should be observed at the positions C24, C25, C45, and C46. Unfortunately, the calculated probabilities of adopting a "reactive" configuration, C45 > C24 > C46 > C25 > C23, are largely inverse to the order of radical stability, which makes it difficult to predict the metabolic regiospecificity in this group with a qualitative approach. In group 1 of everolimus, the situation is similar except that our calculations indicate a higher reactivity for C46 than C45 and no metabolism at C25, which is, however, in contrast to the measurements. Still, our simulations can help identifying metabolism sites that are uncertain from the experimental data. The calculations suggest strongly that only C24 and not C23 are hydroxylated in both substrates. Both 45-OH and C46−OH metabolites should be found to a similar extent in sirolimus while everolimus should be metabolized rather at C46 than at C45.

IV. Summary and Conclusion

Using a mechanism-based approach involving quantum chemical, docking, and molecular dynamics calculations we have studied electronic and orientation effects that influence the metabolic rates of sirolimus and its derivative everolimus, both of which are clinically significant substrates. Our simulations yield good overall qualitative agreement with the measured rate constants[10] for the metabolic groups investigated. In particular, metabolically stable carbon atoms are identified, and the reduction of metabolism upon mutation of sirolimus to everolimus is reproduced. Apart from the qualitative prediction of rate constants, our atom-based simulations allow us to gain insight into substrate/CYP interactions that are important for the metabolism of the substrate. First, our calculations suggest that hydrogen donor functionalities close to the metabolic site and in appropriate relative position to it are important for anchoring the substrate at the catalytic heme center. Replacing this moiety with a hydrophobic group or fluorine atom should reduce the metabolism at this site. Second, we can rationalize why the metabolism in everolimus is considerably reduced compared to sirolimus. Presumably, this is because the hydrophilic hydroxyethyl-chain, which distinguishes everolimus from sirolimus, is forced to distort the compact binding site base of CYP3A4 (group 2) or has other unfavorable interactions with the hydrophobic residues surrounding the heme center (39-O-demethylation).

Although the approach of combining electronic and orientation criteria to predict the metabolism in CYP enzymes has been used before,[17−24] previous applications have focused exclusively on the regiospecificity profile of relatively small substrates with less than 25 non-hydrogen atoms. Our study of sirolimus and everolimus is the first application of this method to considerably larger substrates involving an extensive characterization of several metabolic groups. In contrast to most of the earlier work, in which conclusions about the metabolism of substrates in humans were deduced from simulations on the X-ray model of the bacterial $P450_{cam}$, we use a homology model of the major human cytochrome involved in drug metabolism, CYP3A4. Relying on this 3A4 model, which is based on four bacterial CYP templates, one of which is $P450_{cam}$, should make our conclusions concerning the human metabolism of sirolimus and everolimus more trustworthy than using the $P450_{cam}$ structure alone. In this respect, we should note that Loew et al. have recently used a homology model of human CYP 2C9[23] and 2C18−19[24] for their calculations of preferred hydroxylation sites of different substrates.

Despite the good qualitative results of our modeling efforts, we are aware of the existing shortcomings of our approach. The major limitation is probably the limited structural information of a homology model, which we had to use due to the lack of an X-ray structure of any human CYP. Because of the following reasons, we believe that the 3A4 structural model of this study is accurate enough to justify the qualitative conclusions derived from our simulations. First, regions of the amino acid sequence containing the heme-binding core region are highly conserved in all cytochrome P450s.[39] Second, 3A4 residues that are equivalent to known substrate contact residues of the reference bacterial proteins are located in the active site or the substrate access channel.[14] Last, site-directed mutagenesis studies have confirmed key amino acid residues for substrate binding, which were predicted by the model.[40] Clearly, the incorporation of information from the recently solved X-ray structure of the first mammalian cytochrome P450, 2C5,[41] which shares more sequence similarity with CYP3A4 than the bacterial isoenzymes, should improve the homology model of 3A4 and the accuracy of our calculations.

Another approximation that needs to be commented on is the use of gas-phase calculated energies of the substrate and its corresponding radical intermediate for

estimating the transition state barrier. While this simple approach, due to its computational speed, has been used extensively in previous theoretical studies of product distribution it neglects the effect of the environment on the reaction energetics. However, since we compare the stabilities of radicals the stabilizing effect of the protein on the radical intermediate should be relatively minor and much less so than for charged transition states. Hence, we think that this approach is justified to estimate the electronic effects at each reaction site. Finally, we should note that our calculations rely on the knowledge of the rate-limiting step of the metabolic reaction, which seems to be well established in this case. To compare the theoretical results with experiment, other steps in the reaction process, such as diffusion or product release, must occur on a longer time scale compared to the hydrogen abstraction reaction. Despite those approximations, our results suggest that the simple combination of electronic properties of substrate model compounds and of a geometrical analysis of substrate−enzyme interactions are useful indicators for sites of metabolism.

The good qualitative results of this study suggest the possibility to incorporate the modeling of metabolism at an early stage in the structure based drug design process, thereby reducing the chance of failure at a later and more expensive development phase. One could envision modeling the metabolic activity for the best binding drug candidates and select those which show the desired metabolic profile. Often, groups in the molecule that are likely to be metabolized can be suggested by a pharmacokineticist or predicted using heuristics. Focusing on these groups, the above-mentioned theoretical simulations can yield a qualitative characterization of the metabolic profile and identify problematic metabolic sites. Based on the calculated electronic properties of the drug and the modeled enzyme−substrate interactions one should be able to suggest structural modifications to the drug candidate that would optimize both its metabolic profile and its binding affinity.

Acknowledgment. We would like to thank G. D. Szklarz for kindly providing us with the homology model of cytochrome P450 3A4 as well as S. Toba and A. Verras for helpful discussions. We gratefully acknowledge computer time at the NSF supercomputer centers and graphics support from the UCSF computer graphics lab, T. Ferrin, P. I. (RR-1081). B.K. is grateful for support from the German Academic Exchange Service (DAAD) through a research scholarship. W.J. and L.Z.B. were supported in part by NIH Grant CA72006, and U.C. was supported by the Deutsche Forschungsgemeinschaft, Grant Ch 95/6-2. P.A.K. is pleased to acknowledge research support through the NIH (GM-29072).

Supporting Information Available: Stereoviews of the equilibrated active site structure of the sirolimus/CYP3A4 and everolimus/CYP3A4 complexes. This material is available free of charge via the Internet at http://pubs.acs.org.

References

(1) Kahan, B. D. Efficacy of sirolimus compared with azathioprine for reduction of acute renal allograft rejection: a randomised multicentre study. *Lancet* **2000**, *356*, 194−202.
(2) Sehgal, S. N. Rapamune (Sirolimus, Rapamycin) − an Overview and Mechanism of Action. *Ther. Drug Monit.* **1995**, *17*, 660−665.
(3) Gummert, J. F.; Ikonen, T.; Morris, R. E. Newer immunosuppressive drugs: A review. *J. Am. Soc. Nephrol.* **1999**, *10*, 1366−1380.
(4) Yatscoff, R. W.; Wang, P.; Chan, K.; Hicks, D.; Zimmerman, J. Rapamycin − Distribution, Pharmacokinetics, and Therapeutic Range Investigations. *Ther. Drug Monit.* **1995**, *17*, 666−671.
(5) Sedrani, R.; Cottens, S.; Kallen, J.; Schuler, W. Chemical modification of rapamycin: The discovery of SDZ RAD. *Transplant. Proc.* **1998**, *30*, 2192−2194.
(6) Schuler, W.; Sedrani, R.; Cottens, S.; Haberlin, B.; Schulz, M.; Schuurman, H. J.; Zenke, G.; Zerwes, H. G.; Schreier, M. H. SDZ RAD, a new rapamycin derivative − Pharmacological properties in vitro and in vivo. *Transplantation* **1997**, *64*, 36−42.
(7) Crowe, A.; Bruelisauer, A.; Duerr, L.; Guntz, P.; Lemaire, M. Absorption and intestinal metabolism of SDZ-RAD and rapamycin in rats. *Drug Metab. Dispos.* **1999**, *27*, 627−632.
(8) Benet, L. Z.; Wu, C. Y.; Hebert, M. F.; Wacher, V. J. Intestinal Drug Metabolism and Antitransport Processes − a Potential Paradigm Shift in Oral Drug Delivery. *J. Control. Release* **1996**, *39*, 139−143.
(9) Sattler, M.; Guengerich, F. P.; Yun, C. H.; Christians, U.; Sewing, K. F. Cytochrome-P-450 3a Enzymes Are Responsible for Biotransformation of Fk506 and Rapamycin in Man and Rat. *Drug Metab. Dispos.* **1992**, *20*, 753−761.
(10) Jacobsen, W.; Kuhn, B.; Kollman, P. A.; Christians U.; Benet L. Z. To be submitted for publication.
(11) Lown, K. S.; Mayo, R. R.; Leichtman, A. B.; Hsiao, H. L.; Turgeon, D. K.; SchmiedlinRen, P.; Brown, M. B.; Guo, W. S.; Rossi, S. J.; Benet, L. Z.; Watkins, P. B. Role of intestinal P-glycoprotein (mdr1) in interpatient variation in the oral bioavailability of cyclosporine. *Clin. Pharmacol. Ther.* **1997**, *62*, 248−260.
(12) Lampen, A.; Zhang, Y. C.; Hackbarth, I.; Benet, L. Z.; Sewing, K. F.; Christians, U. Metabolism and transport of the macrolide immunosuppressant sirolimus in the small intestine. *J. Pharmacol. Exp. Ther.* **1998**, *285*, 1104−1112.
(13) Kahan, B. D.; Welsh, M.; Schoenberg, L.; Rutzky, L. P.; Katz, S. M.; Urbauer, D. L.; Vanburen, C. T. Variable Oral Absorption of Cyclosporine − a Biopharmaceutical Risk Factor for Chronic Renal, Allograft Rejection. *Transplantation* **1996**, *62*, 599−606.
(14) Szklarz, G. D.; Halpert, J. R. Molecular Modeling of Cytochrome P450 3A4. *J. Comput.-Aided Mol. Des.* **1997**, *11*, 265−272.
(15) Groves, J. T.; Han, Y.-Z. Models and mechanisms of cytochrome P450 action. *Cytochrome P-450: Structure, Mechanism, and Biochemistry*, 2nd ed.; Plenum Press: New York, 1995; pp 3−48.
(16) Ortiz de Montellano, P. R. Oxygen activation and reactivity. *Cytochrome P-450: Structure, Mechanism, and Biochemistry*, 2nd ed.; Plenum Press: New York, 1995; pp 245−303.
(17) Collins, J. R.; Loew, G. H. Theoretical study of the product specificity in the hydroxylation of camphor, norcamphor, 5,5-difluorocamphor, and pericyclocamphanone by cytochrome P-450cam. *J. Biol. Chem.* **1988**, *263*, 3164−3170.
(18) Collins, J. R.; Camper, D. L.; Loew, G. H. Valproic Acid Metabolism By Cytochrome-P450 − a Theoretical Study of Stereoelectronic Modulators of Product Distribution. *J. Am. Chem. Soc.* **1991**, *113*, 2736−2743.
(19) Paulsen, M. D.; Ornstein, R. L. Predicting the Product Specificity and Coupling of Cytochrome P450cam. *J. Comput.-Aided Mol. Des.* **1992**, *6*, 449−460.
(20) Harris, D.; Loew, G. Prediction of Regiospecific Hydroxylation of Camphor Analogues By Cytochrome P450(Cam). *J. Am. Chem. Soc.* **1995**, *117*, 2738−2746.
(21) Keseru, G. M.; Kolossvary, I.; Bertok, B. Cytochrome P-450 catalyzed insecticide metabolism. Prediction of regio- and stereoselectivity in the primer metabolism of carbofuran: A theoretical study. *J. Am. Chem. Soc.* **1997**, *119*, 5126−5131.
(22) SopkovaDeOliveira, J. S.; Smith, J. C.; Delaforge, M.; Virelizier, H.; Jankowski, C. K. Oxidation of tetrahydro-beta-carboline by cytochrome P-450(cam) − Determination and rationalisation of product distribution. *Eur. J. Biochem.* **1998**, *251*, 398−404.
(23) Payne, V. A.; Chang, Y. T.; Loew, G. H. Homology modeling and substrate binding study of human CYP2C9 enzyme. *Protein-Struct. Funct. Genet.* **1999**, *37*, 176−190.
(24) Payne, V. A.; Chang, Y. T.; Loew, G. H. Homology modeling and substrate binding study of human CYP2C18 and CYP2C19 enzymes. *Protein-Struct. Funct. Genet.* **1999**, *37*, 204−217.
(25) Lee, C.; Yang, W.; Parr, R. G. *Phys. Rev. B* **1988**, *37*, 785.
(26) Becke, A. D. Density-Functional Thermochemistry. 3. the Role of Exact Exchange. *J. Chem. Phys.* **1993**, *98*, 5648−5652.
(27) Stephens, P. J.; Devlin, F. J.; Chabalowski, C. F.; Frisch, M. J. Ab Initio Calculation of Vibrational Absorption and Circular Dichroism Spectra Using Density Functional Force Fields. *J. Phys. Chem.* **1994**, *98*, 11623−11627.

(28) Hehre, W. J.; Radom, L.; van Schleyer, P. R.; Pople, J. A. *Ab Initio Molecular Orbital Theory*; John Wiley: New York, 1986.
(29) Wittbrodt, J. M.; Schlegel, H. B. Some Reasons Not to Use Spin Projected Density Functional Theory. *J. Chem. Phys.* **1996**, *105*, 6574−6577.
(30) Bally, T.; Borden, W. T. Calculations on Open-Shell Molecules: A Beginner's Guide. *Reviews in Computational Chemistry*; Wiley-VCH: New York, 1999; pp 1−97.
(31) Frisch, M. J.; Trucks, G. W.; Schlegel, H. B.; Scuseria, G. E.; Robb, M. A.; Cheeseman, J. R.; Zakrzewski, V. G.; Montgomery, J. A., Jr.; Stratmann, R. E.; Burant, J. C.; Dapprich, S.; Millam, J. M.; Daniels, A. D.; Kudin, K. N.; Strain, M. C.; Farkas, O.; Tomasi, J.; Barone, V.; Cossi, M.; Cammi, R.; Mennucci, B.; Pomelli, C.; Adamo, C.; Clifford, S.; Ochterski, J.; Petersson, G. A.; Ayala, P. Y.; Cui, Q.; Morokuma, K.; Malick, D. K.; Rabuck, A. D.; Raghavachari, K.; Foresman, J. B.; Cioslowski, J.; Ortiz, J. V.; Stefanov, B. B.; Liu, G.; Liashenko, A.; Piskorz, P.; Komaromi, I.; Gomperts, R.; Martin, R. L.; Fox, D. J.; Keith, T.; Al-Laham, M. A.; Peng, C. Y.; Nanayakkara, A.; Gonzalez, C.; Challacombe, M.; Gill, P. M. W.; Johnson, B. G.; Chen, W.; Wong, M. W.; Andres, J. L.; Head-Gordon, M.; Replogle, E. S.; Pople, J. A. *Gaussian 98*; Gaussian, Inc.: Pittsburgh, PA, 1998.
(32) Ewing, T. J. A.; Kuntz, I. D. Critical Evaluation of Search Algorithms for Automated Molecular Docking and Database Screening. *J. Comput. Chem.* **1997**, *18*, 1175−1189.
(33) Cornell, W. D.; Cieplak, P.; Bayly, C. I.; Gould, I. R.; Merz, K. M.; Ferguson, D. M.; Spellmeyer, D. C.; Fox, T.; Caldwell, J. W.; Kollman, P. A. A Second Generation Force Field For the Simulation of Proteins, Nucleic Acids, and Organic Molecules. *J. Am. Chem. Soc.* **1995**, *117*, 5179−5197.
(34) Fox, T.; Kollman, P. A. Application of the RESP Methodology in the Parametrization of Organic Solvents. *J. Phys. Chem. B* **1998**, *102*, 8070−8079.
(35) Bayly, C. I.; Cieplak, P.; Cornell, W. D.; Kollman, P. A. A Well-Behaved Electrostatic Potential Based Method Using Charge Restraints For Deriving Atomic Charges − the Resp Model. *J. Phys. Chem.* **1993**, *97*, 10269−10280.
(36) Giammona, D. A. An examination of conformational flexibility in porphyrin and bulky-ligand binding in myoglobin; University of California at Davis: Davis, CA, 1984.
(37) Ryckaert, J. P.; Cicotti, G.; Berendsen, H. J. C. Numerical Integration of the Cartesian Equations of Motion of a System with Constraints: Molecular Dynamics of *n*-Alkanes. *J. Comput. Phys.* **1977**, *23*, 327−341.
(38) Jorgensen, W. L.; Chandrasekhar, J.; Madura, J.; Impey, R. W.; Klein, M. L. Comparison of Simple Potential Functions for Simulating Liquid Water. *J. Chem. Phys.* **1983**, *79*, 926−935.
(39) Graham, S. E.; Peterson, J. A. How similar are P450s and what can their differences teach us? *Arch. Biochem. Biophys.* **1999**, *369*, 24−29.
(40) Szklarz, G. D.; Halpert, J. R. Molecular basis of P450 inhibition and activation − Implications for drug development and drug therapy. *Drug Metab. Dispos.* **1998**, *26*, 1179−1184.
(41) Williams, P. A.; Cosme, J.; Sridhar, V.; Johnson, E. F.; McRee, D. E. Mammalian microsomal cytochrome P450 monooxygenase: Structural adaptations for membrane binding and functional diversity. *Mol. Cell.* **2000**, *5*, 121−131.

JM010079Y